



Research paper

Combined force decomposition approach and CFD simulation methods for 2D water entry and exit problem

Xupeng Sui^{a,*}, Kamal Djidjeli^a, Zhe Sun^b, Jing Tang Xing^a^a CED Group, Boldrewood Campus, University of Southampton, Southampton, SO16 7QF, UK^b School of Naval Architecture and Ocean Engineering, Dalian University of Technology, Dalian, 116024, China

ARTICLE INFO

Keywords:

Force decomposition
Water entry
Water exit
Computational fluid dynamics

ABSTRACT

The force decomposition approach is extended to solve the two-dimensional (2D) water entry and exit problems. Two typical scenarios, direct water exit and continuous water entry and exit, are examined. It reveals that the total force is irrelevant to the body velocity but to the acceleration. More specifically, the force can be expressed as the multiplication of constant values, body acceleration and a non-dimensional coefficient, and the coefficient is related only to the displacement and immersion condition of the body while independent of its motion condition. Two typical body shapes, a widely used wedge model and a practical ship section model, are examined here. CFD simulation is employed here to directly extract the non-dimensional coefficients, which avoids complex calculations for the wetted length of body by analytical models. The force decomposition approach with the obtained coefficients provides a means to quickly and accurately predict the hydrodynamic force acting on body for water exit scenarios. The proposed method is verified by comparing its results with CFD simulations in the complicated motion cases with varying acceleration. Furthermore, this work provides a potential tool to calculate the total force acting on any entire 3D hull that is divided into several independent 2D slices.

1. Introduction

The study of the water entry and exit problem was motivated by the complex problem of fluid structure interaction (FSI), such as the aircraft ditching and the high-speed craft navigating on the waves. The pioneering work can be traced back to the research of Von Karman (1929). Subsequently, several classical theoretical methods have been proposed based on the Von Karman Model (Von Karman, 1929), including the Original Wagner Model (OWM) (Wagner, 1932), the Modified Logvinovich Model (MLM) (Korobkin, 2004) and the Generalized Wagner Model (GWM) (Zhao et al., 1996).

In recent years, the problem of an elastic body entering or exiting water has attracted increasing attention from researchers. This type of problem is a typical nonlinear fluid-solid interaction problem (NFSIP) involving violent fluid motions and breaking waves, which has been difficult to solve by analytical methods. With the rapid development of computer facilities and various numerical methods, the advanced Computational Fluid Dynamic (CFD) method becomes increasingly popular and is used as an essential and efficient tool to solve such violent NFSIP. Paik et al. (2009) proposed a method to calculate the structural

loads acting on the elastic hull of the S175 container by one-way and two-way coupling of a mesh-based CFD solver with the modal representation of the hull. Using the open-source CFD package OpenFOAM and the volume-of-fluid (VOF) technique, Seng (2012) investigated the whipping and springing response of another elastic container sailing at a constant speed of 15 knots in a head sea. In addition to the traditional CFD methods with mesh distribution, the type of meshless CFD method gradually becomes another powerful and efficient tool to solve complicated hydrodynamic problem. One could be the smoothing particle method with the advantage of simulating breaking wave motions in an accurate way. References (Javed et al., 2016, 2018; Sun et al., 2012, 2013, 2016, 2017, 2019a, 2019b) give some three-dimensional (3D) numerical simulation results using this method, where an aircraft ditching into the water and a ship bottom model dropped on the water surface were investigated. In addition, another mixed finite-element-smoothing particle method described in detail by Xing (2019) had further improved the efficiency of solving problems with strong nonlinear effects. In this paper, however, we are not concerned with the elasticity factor, but focus only on the rigid body.

The 3D numerical approaches mentioned above are undoubtedly

* Corresponding author.

E-mail address: x.sui@soton.ac.uk (X. Sui).<https://doi.org/10.1016/j.oceaneng.2024.117421>

Received 12 January 2024; Received in revised form 24 February 2024; Accepted 6 March 2024

Available online 14 March 2024

0029-8018/© 2024 The Authors. Published by Elsevier Ltd. This is an open access article under the CC BY-NC-ND license (<http://creativecommons.org/licenses/by-nc-nd/4.0/>).

able to provide well-solved results for ship navigating at sea, but involving a large number of particles can be more costly in terms of computational resources. Therefore, researchers have always tried to find some simplified methods to save costs while obtaining solutions accurate enough to satisfy practical applications in naval engineering. In this case, a concept called 'strip theory' (Korvin-Kroukovsky, 1955) has been proposed, where the entire 3D hull is divided into a finite number of 2D transverse slices and can be solved by the potential theory. Through this approximation, the 3D strong nonlinear problem was reduced to a combination of several 2D water entry and exit problems. Subsequently, many researchers have improved this concept to overcome its drawbacks and to extend its scope of application. Some of the work can be found in the available literature (Faltinsen, 2005; Newman, 1964, 2018; Newman and Sclavounos, 1980; Ogilvie and Tuck, 1969; Salvesen et al., 1970).

With regard to the water entry of a 2D rigid body, a state-of-the-art method could be the so-called force decomposition approach originally proposed by Korobkin et al. (2014). In this concept, the total hydrodynamic force acting on the body is decomposed into two components related to the body velocity and acceleration, respectively. Each component was proportional to a specific coefficient that depends only on the displacement of the body, regardless of its state of motion. Their explicit mathematical expressions were derived by Korobkin et al. (2014) based on the basis of various theoretical models of the Wagner-type. However, a drawback of these classical theoretical models was that they were no longer effective for the water entry stage after the flow separation had occurred. Inspired by this, Seng (2012) first tried to directly extract these coefficients from CFD simulations which can also capture the dynamic changes after the flow separation. It was found that the force decomposition approach tended to be ineffective when the body was in a slow motion. Subsequently, Sun et al. (2022) addressed this issue by considering gravity of the fluid into consideration and further applied this approach to the force calculation of bodies with arbitrary shape contours including the asymmetric wedge models and the practical ship section model. This approach was found to greatly facilitate the force prediction and be able to save a large amount of computational time. However, as Sun et al. (2022) commented in his paper, the limitation of the force decomposition approach resulted in it not being applicable to the specific circumstance where the body was in the post-flow separation stage and had a relatively greater deceleration. This paper is partly motivated by a desire to address this limitation.

With respect to the water exit phase, Kaplan (1987, 1992) also divided the total force on the body lifting out of the water into two parts. From the point of view of Kaplan (1987, 1992), these two components can be named as the slamming term and the added mass term, and the slamming term was suppressed during water exit. He indicated that the body acceleration played a dominant role to the hydrodynamic force calculations. Korobkin (2013) applied several assumptions onto the dynamic system and further proposed a linear theoretical resolution to study the flow around the body. As an extension, Korobkin et al. (2017) later applied this linear theory to the body exiting water with a described motion in which the body acceleration varies with time and proposed the developed model which takes into account a certain part of the complicated nonlinear effects. In addition, the body with time-varying shape was also investigated and promising results can be observed from the comparison with the results of direct CFD simulations. Apart from the traditional analytical models above, a kind of semi-analytical model has been proposed by Tassin et al. (2013) using MLM model. The rise of the free surface during the water entry was considered to predict the position of the contact points, and both the acceleration potential and a Kutta condition were applied to such points. However, due to the assumptions introduced, these models may suffer from limited applications that are far away from the real sea conditions. Furthermore, the calculation of the wetted boundary length of the body, which plays a key role in analytical models, tends to be rather complicated and is likely to be time-consuming. In view of these two problems,

numerical methods are used to solve them. One of the works using numerical method is by Del Buono et al. (2021), who proposed a hybrid BEM-FEM approach to combine water entry and exit in order to improve the numerical stability of the resolution, which was verified by the results from other available literature.

In this paper, CFD methods are also used not only to avoid the tedious work of calculating the wetted boundary length of the body, but also to simulate the practical situations. In addition, considering the effectiveness and efficiency of the force decomposition approach demonstrated in Sun et al. (2022), we also aim to extend the force decomposition approach so that it can be applied to the 2D problem with water exit. By combining these advanced methods, the vertical force acting on 2D rigid bodies can be predicted both quickly and accurately. In this case, inspired by the 'strip theory' and then approximately treating the whole 3D hull as a combination of several independent 2D slices, it is an effective way to calculate the force of each slice by using the approach proposed in this paper so that the motion of the 3D hull can be further predicted. In fact, the simplification tends to neglect the influence of the 3D effect, however, the empirical formula concluded by Garne (2005) offers a reliable correction on the force suffered by each section.

Based on the above context, this paper discusses the 2D water entry and exit problem by combining the force decomposition approach and CFD methods. The structure of the paper is organised as follows: first, the theoretical background of the force decomposition approach applied to the water entry and exit problem is presented in Section 2. In Section 3, the CFD strategy to achieve high-fidelity simulation results and the details of different body models used in this research are described. Then, in Section 4, the extraction results of related non-dimensional coefficients for different body models are shown and the performance of the force decomposition approach for force prediction is investigated. Finally, the conclusions are drawn in Section 5.

2. Theoretical background

2.1. Direct water exit

First of all, the analytical models of the direct water exit problem for a 2D rigid and symmetric body, both linear (Korobkin, 2013) and weakly nonlinear (Korobkin et al., 2017), are briefly presented here.

The general sketch of a body vertically lifting out of water is shown in Fig. 1. The origin of the global coordinate system is located at the point where the plane of free surface intersects the vertical axis of symmetry of body. Initially, the fluid is at rest and the body is placed with a certain part below the free surface, represented as the initial immersion depth h_0 . The initial velocity of body is always set as to 0. The end of water exit studied in this paper is at the instant when the bottom point of the body reaches the origin of the coordinate system. c is the half length of the wetted boundary of body projected on the horizontal axis.

Starting from the linear model, some of the assumptions are described below: (i) the deadrise angle of body is small and the curvature of any point within the body boundary is much less than 1; (ii) gravity, surface tension and fluid viscosity are all excluded; (iii) the acceleration of body is much greater than the gravitational acceleration $|g|$ ($|g| = 9.8 \text{ m/s}^2$); (iv) the duration of water exit is much shorter; (v) the cavitation phenomenon never occurs. More detailed information can be found in the work of Korobkin (2013) and Korobkin et al. (2017). In this case, if the vertical velocity of body is much slower than the rate of change of the half length of the wetted boundary (i.e. \dot{c}), it is reasonable to assume that the boundary conditions for both the free surface and the wetted part of body can be linearized, which is similar to the treatment of the water entry problem within the OWM model (Wagner, 1932). In this case, the velocity potential ϕ of flow satisfies the following boundary conditions:

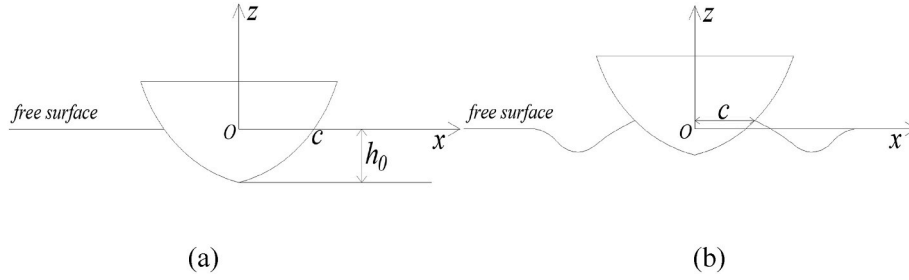


Fig. 1. Sketch of direct water exit for a 2D rigid and symmetric body (a) The initial condition; (b) At some instant.

$$\begin{cases} \Delta\varphi = 0 & (z < 0) \\ \varphi_t = 0 & (z = 0, |x| > c(t)) \\ \varphi_z = v(t) & (z = 0, |x| < c(t)) \\ \varphi \rightarrow 0 & (x^2 + z^2 \rightarrow \infty) \end{cases} \quad (1)$$

where h and $v = dh/dt$ are the dimensional displacement and the vertical upwards velocity of body. It is obvious that the boundary conditions of the velocity potential φ are identical for both water entry and exit problems. However, as noted by Korobkin (2013), it is inappropriate to simply treat water exit as an inverse entry problem. Specifically, as suggested by Korobkin (2013) and Korobkin et al. (2017), c is instead calculated by the following equation:

$$\frac{dc}{dt} = \gamma\varphi_x(c(t), 0, t) \quad (2)$$

where γ is an indeterminate coefficient that varies with the shape of body. For example, it is chosen by Korobkin (2013) and Korobkin et al. (2017) to be 2 for a given body model by Piro and Maki (2011). In fact, the total force acting on the body is independent of the value of γ , which has been verified by Korobkin (2013) and Korobkin et al. (2017).

Within the linear dynamic system, the pressure distribution along the wetted boundary of body can be calculated by the linear Bernoulli equation $P(x, z, t) = -\rho\varphi_t$. Following the treatment of Korobkin (2013), where the flat-disc approximation was applied to the wetted part of blunt bodies and the calculation of pressure was placed on the plane of free surface, i.e. $z = 0$, the formula for the pressure distribution along the body wetted boundary can be expressed as follows:

$$P(x, 0, t) = -\rho a(t)\sqrt{c^2(t) - x^2} \quad (|x| < c(t)) \quad (3)$$

where a is the acceleration of body (positive if accelerating upwards). It is easy to see from Eq. (3) that the solution of c from Eq. (2) plays an important role in the computation of the pressure distribution. Unfortunately, there are few explicit expressions of c from the available literature.

Furthermore, inspired by the ideas from MLM (Korobkin, 2004) and GWM (Zhao et al., 1996) models for the water entry problem, Korobkin et al. (2017) considered the non-linear factors. The pressure distribution was then calculated at the real position of the wetted boundary instead of the plane of free surface. Apart from that, the original nonlinear Bernoulli equation was used and expressed as

$$P(x, z_b(x, t), t) = -\rho \left(\varphi_t - \frac{z_{b,t}z_{b,x}}{1+z_{b,x}^2}\varphi_x + \frac{1}{2} \frac{\varphi_x^2 - z_{b,t}^2}{1+z_{b,x}^2} \right) \quad (4)$$

where z_b is the body shape function; $z_{b,t}$ and $z_{b,x}$ are the derivatives with respect to time and horizontal position, respectively. As suggested by Korobkin et al. (2017), the terms with φ_x and $y_{b,x}^2$ can be neglected due to the blunt contour of body. Consequently, the pressure distribution along of the body wetted boundary can be finally formulated as

$$P(x, z_b(x, t), t) = -\rho a(t)\sqrt{c^2 - x^2} - \rho \left(a(t)(z_b(x, t) - z_b(c, t)) - \frac{1}{2}v^2(t) \right) \quad (5)$$

Considering one of the aforementioned assumptions, the entire water exit process will never last for a long period of time, in which case the velocity of body will always be in a small quantity and contribute little to the pressure calculation. Consequently, the pressure component related to the velocity of body is ignored in our paper and subsequently the pressure at any point within the wetted boundary can be approximately expressed as proportional to one specific coefficient by

$$P(x, t) = \rho a(t)P_a(x, t) \quad (6)$$

where $P_a(x, t) = -\sqrt{c^2 - x^2} - z_b(x, t) + z_b(c, t)$ represents the pressure coefficient and is independent of the motion state of body if its shape is given. If we replace the displacement of body with time as the variable representing the time domain, then Eq. (6) can be rewritten as

$$P(x, h) = \rho a(h)P_a(x, h) \quad (7)$$

If we further perform non-dimensionalisation on these coefficients, Eq. (7) can be presented as the following equation:

$$P(\sigma, \xi) = \rho a(\xi)h_0P_A(\sigma, \xi) \quad (8)$$

where $\xi = h/h_0$ is the non-dimensional displacement with $\xi \in [0, 1]$, $\sigma = x/c$ is the non-dimensional horizontal coordinate with $\sigma \in [0, 1]$ also, and $P_A(\sigma, \xi) = P_a(x, h)/h_0$ is the non-dimensional pressure coefficient which is not yet affected by the motion state of body.

Accordingly, the total force acting on the body can be computed by integrating the pressure distribution Eq. (8) along the body wetted boundary, which can be formulated as

$$F(\xi) = 2 \int_0^1 P(\sigma, \xi) d\sigma = 2 \int_0^1 \rho a(\xi)h_0P_A(\sigma, \xi) d\sigma = \rho a(\xi)h_0^2F_A(\xi, h_0) \quad (9)$$

$$F_A(\xi, h_0) = \frac{2 \int_0^1 P_A(\sigma, \xi) d\sigma}{h_0} \quad (10)$$

where F_A is the non-dimensional force coefficient, which is also independent of the body motion state.

Observing the formula for the resolution of the total force acting on body, i.e. Eq. (9), it can be seen that this equation provides an alternative perspective to solve the direct water exit problem by calculating the corresponding non-dimensional coefficient, if we are not concerned with the details of the flow around the body boundary. In this case, the attention should be focused on calculating the half width of the wetted boundary c . However, as mentioned above, it is usually difficult to solve by using theoretical methods. In this paper, instead of putting much effort into obtaining the explicit formula of the non-dimensional coefficient F_A , we will directly extract this coefficient by performing high-fidelity CFD simulations. The extraction procedure is inspired by the work of Sun et al. (2021). In detail, after obtaining CFD simulation results for one case where the body is given a described motion with

constant acceleration, the evolution of the non-dimensional force coefficient F_A against the non-dimensional displacement of the body ξ can be described by solving the following equation:

$$F_A(\xi, h_0) = \frac{F(\xi)}{\rho a h_0^2} \quad (11)$$

Considering that the motion state of body does not influence the extraction results of F_A , consisting of the expression of Eq. (11), it can be expected that if the body shape and the initial immersed depth are specified in advance, the total force acting on it at any time during water exit can be quickly calculated by using the force decomposition approach together with the previously obtained F_A .

2.2. Continuous water entry and exit

In this subsection, we will first introduce the force decomposition approach to solve the continuous water entry and exit problem. Further details on the derivation of the force decomposition approach can be found in Appendix A.

The general outline of this problem can be seen in Fig. 2. Specifically, the body also moves in the vertical direction represented by the z axis and time starts to be counted at the instant when the bottom point of the body touches the calm free surface. The body is given an initial downward velocity and an upward acceleration. The water entry stage ends when the velocity of body decreases to zero and the body has reached the maximum depth of immersion h_m , while the water exit stage stops when the body returns to its initial position. Furthermore, at the end of the water entry stage, the upper boundary of body remains as dry as at the beginning, indicating that the entire body will never be below the free surface.

If we assume that the gravity of the fluid is not considered and the boundary conditions Eq. (1) govern the velocity potential of flow ϕ for both water entry and exit stages, then the OWM model produces the equation for calculating the total force acting on the body, which is shown as below:

$$F(h) = \rho \pi v^2(h) c \frac{dc}{dh} + \rho \frac{\pi}{2} a(h) c^2(h) \quad (12)$$

Here, the total force is divided into two different components, and the component proportional to the square of the velocity of body $v(h)$ is called the slamming term, while the component proportional to the acceleration of body $a(h)$ is called the added mass term. Here, c is determined by the location of the root of jet, which can be solved according to the well-known Wagner condition (Korobkin, 1996).

Following a similar practice carried out in the previous subsection,

another two non-dimensional coefficients are introduced here, and then Eq. (12) can be rewritten as

$$F(\xi) = \rho v^2(\xi) h_m F_V(\xi, h_m) + \rho a(\xi) h_m^2 F_W(\xi, h_m) \quad (13)$$

where F_V and F_W are the nondimensional velocity and acceleration-related coefficients, respectively. It should be noted that ξ falls in the range interval $[0,1]$ when the body is experiencing the water entry stage, while it falls in the range interval $[1,2]$ when the body is in the water exit stage. In addition, it can be seen that, similar to, F_A , both of these coefficients depend only on the body displacement and its maximum immersed depth, regardless of the motion state.

The procedure for the extraction of F_V and F_W also refers to the work of Sun et al. (2022). In detail, the extraction of F_V can be carried out from simulations with body having the constant velocity while the extraction of F_W from simulations with body having the constant acceleration. In fact, considering the body is given a specific constant acceleration and under the premise that the body is certain to experience the moment when its velocity is 0 and displacement is h_m , the square of the instantaneous velocity of body can be written as $v^2 = 2ah_m(1 - \xi)$. In this case, the calculation of the total force can be further expressed as

$$\begin{aligned} F(\xi) &= \rho(2ah_m - 2ah_m\xi)h_m F_V(\xi, h_m) + \rho ah_m^2 F_W(\xi, h_m) \\ &= 2\rho a(1 - \xi)h_m^2 F_V(\xi, h_m) \\ + \rho ah_m^2 F_W(\xi, h_m) &= \rho ah_m^2 (2F_V(\xi, h_m) - 2\xi F_V(\xi, h_m) + F_W(\xi, h_m)) \\ &= \rho ah_m^2 F_\alpha(\xi, h_m) \end{aligned} \quad (14)$$

where $F_\alpha(\xi, h_m) = 2F_V(\xi, h_m) - 2\xi F_V(\xi, h_m) + F_W(\xi, h_m)$ is a new non-dimensional coefficient. It can be observed from Eq. (14) that the total force acting on the body during continuous water entry and exit is proportional to the exact value of the acceleration. Following the same procedure as in Section 2.1, we can obtain the profile of F_α by the following equation:

$$F_\alpha(\xi, h_m) = \frac{F(\xi)}{\rho ah_m^2} \quad (15)$$

It should be noted that although the extraction of F_α is based on the assumption that the body is always under the constant acceleration situation, it has already been verified that the complicated cases with the varying acceleration are also included and the corresponding results are shown in Section 4.5. Some related evidence can be found in the work of Sun et al. (2022) as well.

The high-fidelity force information $F(\xi)$ required in Eq. (15) is still collected from the CFD simulation database. The CFD strategy used in this research is described in detail in the next section.

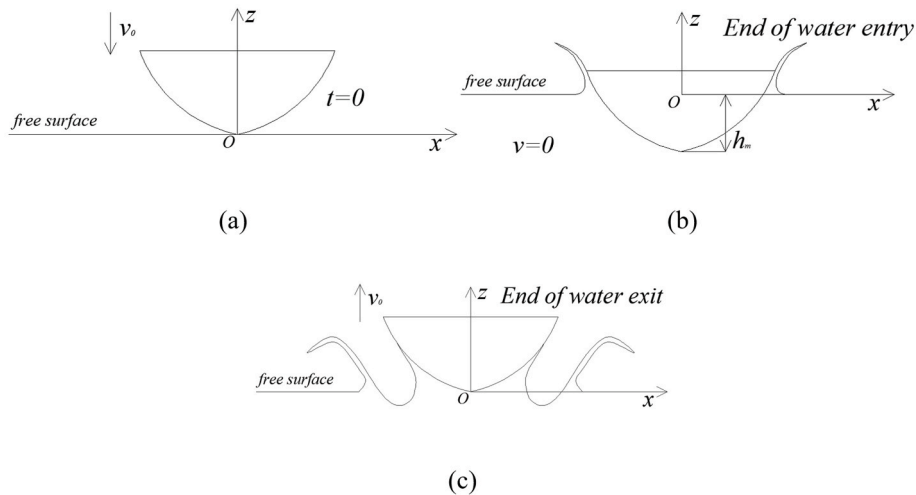


Fig. 2. Sketch of continuous water entry and exit for a 2D rigid and symmetric body (a) The initial condition; (b) At the end of water entry; (c) At the end of water exit.

3. Computational Fluid Dynamics strategy

3.1. CFD models

The STAR-CCM+ software is used to perform numerical simulations, from which the high-fidelity results of the total force acting on the body can be obtained. The work of Sun et al. (2022), where the force decomposition approach was also investigated with the help of STAR-CCM+ software, provides us with much inspiration for both physical model selection and CFD solver settings. Therefore, given the success of their work, we followed a similar approach in terms of CFD strategy.

More specifically, in all cases, the Reynolds-Averaged Navier-Stokes (RANS) model is used to solve the governing equations while the VOF technique is employed to capture the dynamic changes of free surface between the air and the water phases. As the body remains at a low velocity for most of the process and the total duration time of its movement is not long, the Reynold number won't be a large value and the time scale is too short for a turbulent flow to develop (Tassin et al., 2013), in which case the laminar model is accurate enough for numerical simulation of water exit. However, in order to be close to the real maritime situations, the turbulence model is still used for all simulation cases. Specifically, the realizable $k - \epsilon$ model is chosen because the fluid viscosity is too weak to be considered in the problem we are investigating, and this model can provide relatively more flexibility compared to the standard $k - \epsilon$ model. In addition, the gravity of the fluid is never taken into account.




Two typical types of 2D rigid and symmetric body models are extensively investigated in our work. One is the widely used wedge model, while the other is the practical ship section model derived from the work of Aarsnes (1996). Meanwhile, a test model is also included for the convergence study and the accuracy verification of the force decomposition approach. Detailed shape and dimension information for all models are shown in Table 1.

The dynamic system for each model is then solved by using the finite volume method. A sketch of the computational domain is shown in Fig. 3, using the wedge model A for instance. Here, the boundary conditions for the side and bottom boundaries of the entire domain are rigid walls, while the pressure at the top is set to be constant, i.e., the standard atmosphere. Detailed computational domain dimensions for each body model in Table 1 are listed in Table 2.

In order to achieve the simulation results with a high level of accuracy while keeping the computational cost acceptable, the multi-resolution meshing strategy is used. Meantime, the overset mesh approach is used around the moving body to couple other parts of the domain in an arbitrary but feasible way. In general, for each model, the entire computational domain is divided into four different regions: Background, Free Surface, Refining and Overset, respectively. In addition, the prism layer with a total number of 10 is placed along the boundary of each model. It should be noted that the mesh size, as well as the thickness of the prism layer, varies with the shape of the body model.

Taking the ship section model directly lifting out of the water as an

Table 1
Detailed shape and dimension information for different body models.

Model	Shape and Size	Sketch	Notes
Wedge model A	1 m half-width and 30-deg deadrise angle		
Ship Section model	0.36 m half-width and 0.4627 m height		Profiles refer to Aarsnes (1996)
Wedge model B	0.5 m half-width and 10-deg deadrise angle		Used for the convergence study and the verification only

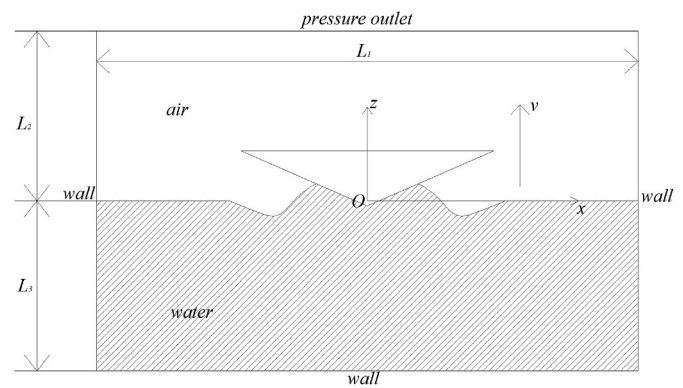


Fig. 3. Sketch of computational domain for the wedge model A.

Table 2
Computational domain dimensions for each body model.

Models	L_1	L_2	L_3
Wedge model A	30 m	7 m	7 m
Ship section model	15 m	5 m	5 m
Wedge model B	12 m	3 m	3 m

instance, the mesh distribution is elaborated as follows. Firstly, the computational domain is discretised by a specific type of structured meshes called 'trimmed cell meshes' provided by STAR-CCM+, whose shapes are square or rectangle for 2D simulations. Secondly, the overall layout is shown in Fig. 4, and it is easy to see that the meshes around the body and the free surface are refined, while the meshes away from the region of interest are gradually sparsely distributed. More specifically, if we introduce the parameter H as the height of the ship section, the mesh size of different regions can be approximately represented as $50\% H^*$ $50\% H$ for Background, $6.25\% H^*$ $3.125\% H$ for Free Surface, $12.5\% H^*$ $6.25\% H$ for Refining, and $1.5625\% H^*$ $1.5625\% H$ for Overset, respectively, and the total thickness of the prism layers is $8\% H$. A similar meshing strategy as mentioned above is applied to other models, either in the direct water exit or in the continuous water entry and exit, if not specified.

In addition, the time step should also vary with different motion conditions. Here, as a brief illustration, the exact value of the time step is chosen to ensure that the Courant number always meets the Courant–Friedrichs–Lewy (CFL) condition throughout the entire process, i.e. kept below 1. The machine used to run all simulations is a Windows-based computer with a Core i5-12500 processor having 6 cores and a speed of 3.0 GHz and 16 GB of RAM. The computational time varies for different scenarios and is given at the beginning of each subsection in Section 4.

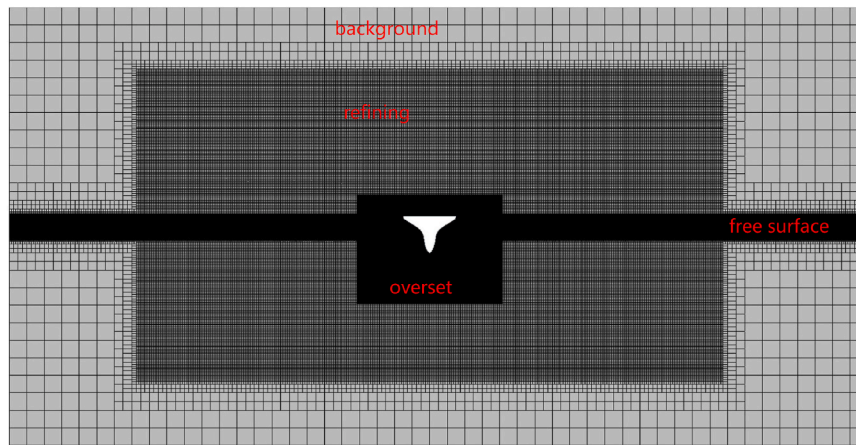
In summary, in order to allow all simulation cases to be easily replicable for future readers, detailed information on the setups in STAR-CCM+ is listed in Table 3.

3.2. Convergence study and verification

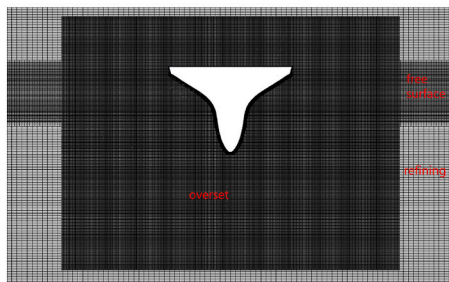
To check the validity and accuracy of simulation cases using the turbulence model and the meshing strategy introduced in Section 3.1, the wedge model B is used for investigation.

Specifically, the body experiences a continuous water entry and exit and is given an imposed motion case with an initial downward speed of 4 m/s and a constant upward acceleration of 181.48 m/s². Further details can be found in the work of Piro and Maki (2011).

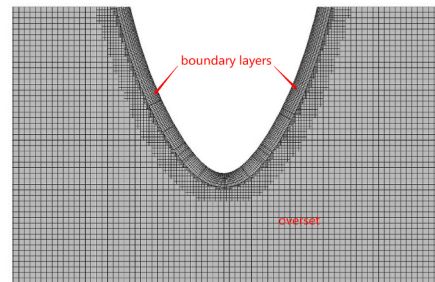
In addition, to check the convergence of our results, three different sets of mesh sizes are used, which are named as Coarse mesh, Current mesh and Fine mesh. The dimension of each set is represented by the mesh size of the overset region: $2.0 \times 2.0 \text{ mm}^2$, $1.5 \times 1.5 \text{ mm}^2$ and $1.0 \times$



(a)



(b)



(c)

Fig. 4. Mesh distribution for the ship section model (a) The overall distribution; (b)–(c) Zoomed parts.

Table 3
Information on the setups in STAR-CCM+.

Problem investigated	Physical models and techniques		
2D rigid body vertically entering and exiting water.	<ul style="list-style-type: none"> ● RANS model. ● Multiphase interaction model. ● VOF technique. ● Realizable $k - \epsilon$ model. ● Overset mesh technique. <p>Mesh distribution</p> <ul style="list-style-type: none"> ● Mesh type: Trimmed cell meshes (Structured meshes). ● Reference level: Free water surface. ● Discretization schemes: Finite volume method. ● Prism layer around the body surface: 10 layers with a stretching ratio of 1.2. ● Basic principle: Becoming sparser as mesh away from the body model. <table border="0" style="width: 100%;"> <tr> <td style="vertical-align: top;"> <p>Time step</p> <ul style="list-style-type: none"> ● Satisfying that the Courant number is below 1. </td> <td style="vertical-align: top;"> <p>Convergence criteria</p> <ul style="list-style-type: none"> ● 10 inner iterations within a single time step. </td> </tr> </table>	<p>Time step</p> <ul style="list-style-type: none"> ● Satisfying that the Courant number is below 1. 	<p>Convergence criteria</p> <ul style="list-style-type: none"> ● 10 inner iterations within a single time step.
<p>Time step</p> <ul style="list-style-type: none"> ● Satisfying that the Courant number is below 1. 	<p>Convergence criteria</p> <ul style="list-style-type: none"> ● 10 inner iterations within a single time step. 		

1.0 mm² are for Coarse, Current and Fine mesh respectively.

These three cases are then run numerically in STAR-CCM+ and force predictions versus time are extracted directly from the simulation results. Fig. 5 shows the comparison between the results of STAR-CCM+ and from the work of Piro and Maki (2011). Here, another parameter of the non-dimensional force is introduced, expressed as

$$f = \frac{F}{0.5\rho\left(\frac{v_e}{2}\right)^2 B} \tag{16}$$

$$v_\eta = \begin{cases} 0.5v_e & \text{for direct water exit} \\ 0.5v_0 & \text{for continuous water entry and exit} \end{cases} \tag{17}$$

where B is the half width of body and v_e is the velocity of body at the end of the direct water exit.

It can be seen from Fig. 5 that the results of the case with a relatively coarse mesh size show some obvious differences compared to those with the current mesh size, especially during the water exit stage. On the other hand, when the mesh size has a denser distribution, the results obtained show little variation and have a good agreement with the current mesh size case, indicating that the converged results are achieved. Furthermore, the converged results also show a fairly good agreement with those by Piro and Maki (2011). Therefore, it can be concluded that our physical model selection and meshing strategy used for the numerical simulation have been verified and can provide accurate and reliable enough predictions for the problem discussed in this paper.

4. Results and discussion

In this section, some extraction results of the non-dimensional coefficients F_A and F_a for different body models will be shown. For each of the typical scenarios, i.e., the direct water exit and the continuous water entry and exit, the wedge model A and the ship section model are respectively given different motion cases featured with constant accel-

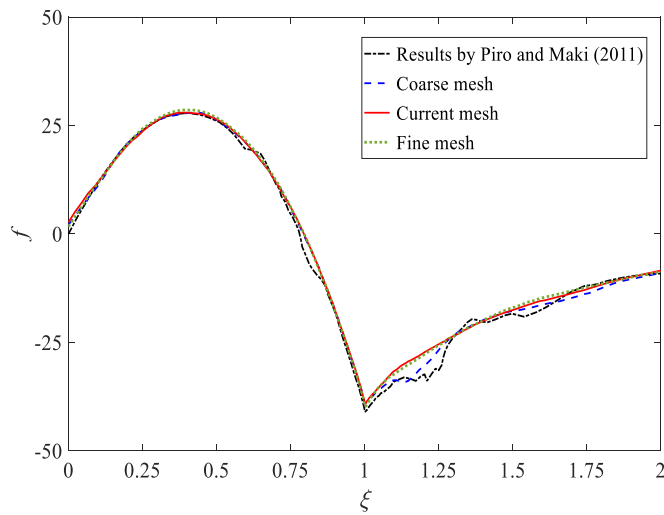


Fig. 5. Convergence study for the selected physical model and meshing strategy.

eration. The detailed information of the motion cases, the extraction results of $F_A(\xi)$ and $F_\alpha(\xi)$, and the corresponding analysis can be found in the following subsections. In addition, in the last subsection, the applicability of the force decomposition approach is further investigated by simulating more complicated motion cases where the acceleration of body varies with time.

4.1. Direct water exit for the wedge model

First of all, the direct water exit of the wedge model A is examined. A total of nine motion cases, numbered from 1 to 9, are given to this model, as shown in Table 4. In these motion cases, the body is lifted directly out of water with three different constant accelerations, placed with three different initial immersed depths. The total computational time to run each simulation is approximately 3.3 core hours.

After numerically simulating each case in the CFD software STAR-CCM+ and then obtaining information about the total force acting on the body, the non-dimensional coefficient F_A is extracted using Eq. (11). Fig. 6 shows the detailed profile of this coefficient as it varies with the non-dimensional displacement ξ under all the motion cases. Each type of line/symbol represents for the specific cases with the same constant acceleration while each colour represents those with the same

Table 4
Detailed information on motion cases for the wedge model A under direct water exit.

Model	Case No.	Motion condition ($v_0 + at$)	Immersion condition
Wedge model A	1	$0 + 8 g t$ m/s	0.55 m initial immersed depth
	2		0.45 m initial immersed depth
	3		0.35 m initial immersed depth
	4	$0 + 5 g t$ m/s	0.55 m initial immersed depth
	5		0.45 m initial immersed depth
	6		0.35 m initial immersed depth
	7	$0 + 2 g t$ m/s	0.55 m initial immersed depth
	8		0.45 m initial immersed depth
	9		0.35 m initial immersed depth

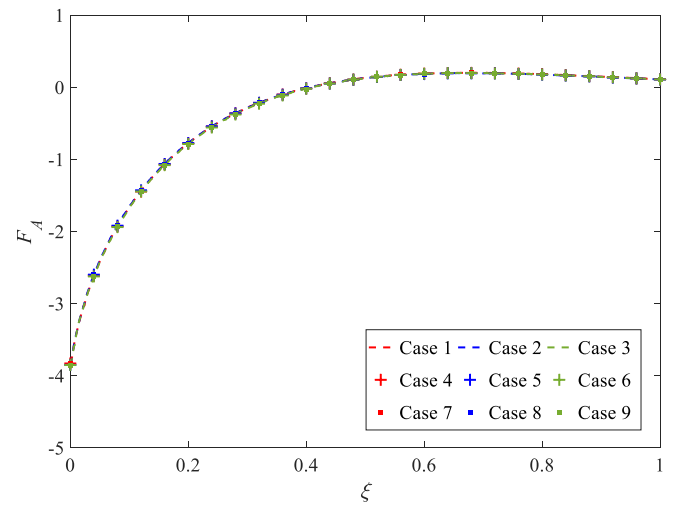


Fig. 6. Coefficient F_A for the wedge model A. (The specific type of line/symbol represents for the cases with the same constant acceleration while the specific colour represents those with the same immersion condition.)

immersion condition. It is interesting to note from Fig. 6 that all the extracted F_A are in perfect agreement with each other. With respect to the evolution tendency of $F_A(\xi)$, it can be seen that at the beginning of the direct water exit, the body experiences a considerable hydrodynamic force from the water pulling it downwards and relatively weak supporting force during the second half of the exit process. More specifically, at the moment when the body's non-dimensional displacement ξ is about 0.4, the direction of the total force changes from downwards to upwards and then remains the same until the end. In addition, the total force always has an increasing tendency for most of the water exit process, while showing a slight decrease towards the end.

It can be concluded that the coefficient F_A is a function that depends only on the displacement of body and is never affected by the motion state and the initial immersed depth of the body, i.e. $F_A = F_A(\xi)$. In other words, the particular curve representing F_A , shown in Fig. 6, can be used for further prediction of the total force acting on this wedge body, whatever state of motion it is in. Furthermore, it can be expected that the above conclusion is also applicable to any wedge model with other shape sizes, such as the wedge model B.

4.2. Continuous water entry and exit for the wedge model

The continuous water entry and exit for the wedge model A is then examined in this subsection. Firstly, it should be noted that during the water entry process, the elevation of water around the body boundary will lead to a well-known phenomenon called flow separation when the root of jet reaches the edge of the body contour. For the most of the available models, the water entry problem before the occurrence of flow separation can be easily solved by using these models, but unfortunately, they are no longer effective at the later stage of water entry. To solve this problem, some numerical methods have been proposed, such as the work of Sun et al. (2022), using CFD methods together with the force decomposition approach. However, it was pointed out by Sun et al. (2022) that there are some limitations that prevent the application of this concept to be applied to specific circumstances. Specifically, when the body is in the entry motion with a large deceleration, the force decomposition approach cannot provide accurate force prediction after the flow separation occurs. Based on the context mentioned above, we shall further investigate the force decomposition to solve the above limitation, together with further application of this concept to the force prediction during the following water exit stage. Therefore, this subsection is divided into two different parts depending on whether the flow separation occurs or not.

(1) With flow separation

Considering that the flow separation has already occurred at the moment when the velocity of body decreases to zero and the water exit movement is about to start, another nine different motion cases are given to this wedge model. Specifically, the values of constant acceleration are still $8|g|$, $5|g|$ and $2|g|$ m/s^2 and the wedge reaches three different maximum penetration depths at the end of water entry, i.e., 0.55, 0.5 and 0.45 m. Further details are given in Table 5 below. It takes around 7.7 core hours to simulate each case.

Following the same practice conducted in Section 4.1, the results of the non-dimensional coefficient F_α under different motion cases are extracted from CFD simulations, which are shown in Fig. 7. It is clear to see that although the evolution of F_α continues to be independent of the motion state of body, the initial immersion condition has a great influence on its profile, which can be observed by distinguishing different colours of the results. In detail, the discrepancy appears roughly at $\xi = 0.65$ and all results return to good agreement after $\xi = 1.5$. Despite the obvious discrepancies with respect to the value in the middle period of the entire continuous water entry and exit process, the tendencies of the extracted F_α remain in a coincidence, i.e., the total force first decreases to a negative extreme point and then increases to almost zero. Meantime, the body tends to experience a relatively greater pulling hydrodynamic force under the condition of smaller maximum penetration depths.

To briefly summarise, in the cases where the flow separation occurs at the water entry stage, apart from the displacement of body, the maximum penetration depth is another crucial factor affecting the non-dimensional coefficient F_α , which indicates $F_\alpha = F_\alpha(\xi, h_m)$. In this case, if the size of wedge and its maximum penetration depth are specified in advance, we can run a high-fidelity numerical simulation only once to obtain the corresponding curve of F_α variation with displacement. Then, further force prediction under the identical condition of maximum penetration depth can be provided in a fast and accurate way by using the force decomposition approach and the previously obtained F_α , without performing extensive numerical simulations or mathematical calculations. Although not fully solved, the limitation of the force decomposition approach is greatly reduced when it is applied to the water entry of a body with a deceleration motion condition.

(2) Without flow separation

A total of six motion cases without the occurrence of flow separation during the water entry stage are given to the wedge model A. The

Table 5
Detailed information on motion cases for the wedge model A under continuous water entry and exit with flow separation.

Model	Case No.	Constant acceleration	Immersion condition
Wedge model A	10	$8 g $ m/s^2	0.55 m maximum penetration depth
	11		0.5 m maximum penetration depth
	12		0.45 m maximum penetration depth
	13	$5 g $ m/s^2	0.55 m maximum penetration depth
	14		0.5 m maximum penetration depth
	15		0.45 m maximum penetration depth
	16	$2 g $ m/s^2	0.55 m maximum penetration depth
	17		0.5 m maximum penetration depth
	18		0.45 m maximum penetration depth

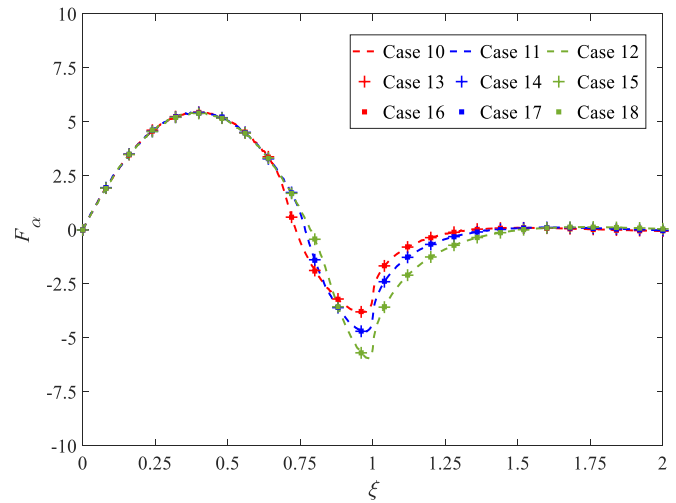


Fig. 7. Coefficient F_α for the wedge model A with flow separation. (The specific type of line/symbol represents for the cases with the same constant acceleration while the specific colour represents those with the same immersion condition.)

selected values of constant acceleration remain unchanged, but the body will have a smaller proportion of the body immersed below the free surface at the end of water entry. The details of these six cases are given in Table 6. Approximately 6.7 core hours are required to run each single simulation.

The extractions of F_α corresponding to each motion case in Table 6 are described in Fig. 8. It has been verified by Sun et al. (2022) that the water entry without flow separation falls outside the limitation of the force decomposition approach. Therefore, it is not surprising to find that when there is no flow separation, the non-dimensional coefficient F_α within the water entry process, i.e. $\xi \in [0, 1]$, is still a function related only to the displacement of body. Meanwhile, it is interesting to note that the results of F_α from the water exit stage, i.e. $\xi \in [1, 2]$, are also in perfect agreement. In this case, similar to the procedure of how the coefficient F_A is used for the direct water exit problem, accurate predictions of the total force acting on the body in continuous water entry and exit can be provided by using the force decomposition approach and the unique previously extracted F_α , regardless of the motion state and the maximum penetration depth of body.

4.3. Direct water exit for the ship section model

Next, the applicability of the force decomposition approach to bodies with more complicated shape contours is investigated, focusing on the practical ship section model. First, the direct water exit process is considered. The ship section model is given a total of nine motion cases

Table 6
Detailed information on motion cases for the wedge model A under continuous water entry and exit without flow separation.

Model	Case No.	Constant acceleration	Immersion condition
Wedge model A	19	$8 g $ m/s^2	0.35 m maximum penetration depth
	20		0.3 m maximum penetration depth
	21	$5 g $ m/s^2	0.35 m maximum penetration depth
	22		0.3 m maximum penetration depth
	23	$2 g $ m/s^2	0.35 m maximum penetration depth
	24		0.3 m maximum penetration depth

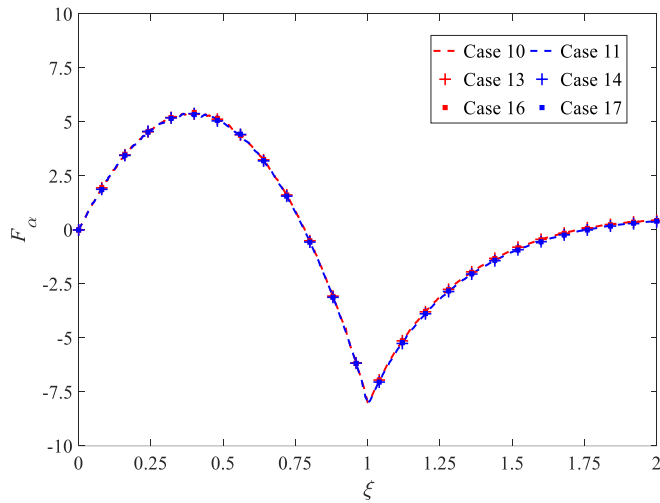


Fig. 8. Coefficient F_α for the wedge model A without flow separation. (The specific type of line/symbol represents for the cases with the same constant acceleration while the specific colour represents those with the same immersion condition.)

consisting of three different constant accelerations, i.e. $8|g|$, $5|g|$ and $2|g|$ m/s^2 , and three different initial submerged depths, i.e. 0.45, 0.35 and 0.25 m. Details of these motion cases are given in Table 7. The total computational time to run each simulation is approximately 4.2 core hours.

Similarly, the results of the non-dimensional coefficient F_A are subsequently extracted from the CFD simulation database and are shown in Fig. 9. Contrary to those of the wedge model A, the profiles of F_A for the ship section model are greatly affected by the initial immersed depth, which are represented with different colours, indicating $F_A = F_A(\xi, h_0)$. The aforementioned difference between these two different body shapes reveals that it is the complexity of the hull contour that accounts for it. However, it is also a promising finding that the motion state of body still has little influence on F_A . Moreover, by observing the similar evolution tendency of curves corresponding to different immersion conditions, if we further carry out manual scale and translation conducts on both lateral and vertical dimensions of these curves, it can be found that they have an interesting coincidence with each other and become independent of the immersion condition, which shows in Fig. 10. To avoid confusion, we further introduce ξ' and F_A' as variables of ξ and F_A after

Table 7

Detailed information on motion cases for the ship section model under direct water exit.

Model	Case No.	Motion condition ($v_0 + at$)	Immersion condition
Ship section model	25	$0 + 8 g t$ m/s	0.45 m initial immersed depth
	26		0.35 m initial immersed depth
	27		0.25 m initial immersed depth
	28	$0 + 5 g t$ m/s	0.45 m initial immersed depth
	29		0.35 m initial immersed depth
	30		0.25 m initial immersed depth
	31	$0 + 2 g t$ m/s	0.45 m initial immersed depth
	32		0.35 m initial immersed depth
	33		0.25 m initial immersed depth

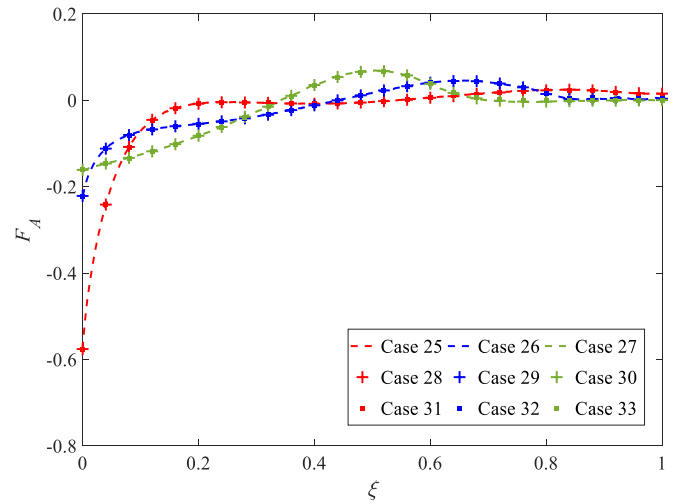


Fig. 9. Coefficient F_A for the ship section model. (The specific type of line/symbol represents for the cases with the same constant acceleration while the specific colour represents those with the same immersion condition.)

the aforementioned transformations. It can be seen from Fig. 10 that for the curves corresponding to the cases with 0.35 m and 0.25 m immersion condition, the non-dimensional displacement of body no longer falls into the interval $[0,1]$, which indicates that the immersion condition probably does not affect the evolution pattern of the flow around the body but the rate and starting/ending moment within the entire evolution process.

Furthermore, considering that it may be a tedious task to solve such direct water exit problems by theoretical models, using the force decomposition approach seems to be more advantageous because a large amount of computational time can be saved if the body shape contour and the initial immersed depth are determined in advance. Meanwhile, we also do not need to pay attention to the details of the flow around the body boundary but to the acquisition of F_A , which can be obtained easily by using numerical methods.

4.4. Continuous water entry and exit for the ship section model

In this subsection, the results of the extraction of the non-dimensional coefficient F_α for the ship section model experiencing continuous water entry and exit are examined. Depending on the occurrence of flow separation, this subsection is divided into two parts, the rationale of which has been explained in Section 4.2. The detailed discussion is presented below.

(1) With flow separation

A total of nine motion cases with different constant accelerations are given to the ship section model, counting from case 34 to 42. The values of constant acceleration are still $8|g|$, $5|g|$ and $2|g|$ m/s^2 while the penetration depths of the ship section at the end of water entry are 0.45, 0.4 and 0.35 m. In each case the flow separation occurs during the water entry phase. Further information is given in Table 8. It takes around 9.4 core hours to simulate each case.

The extracted results of F_α for the ship section model are shown in Fig. 11. It is found that the discrepancies between the results under different motion cases can be observed from the range interval of $\xi \in [0.4, 1.3]$, which is caused by the variation of the maximum penetration depth. However, the evolution of F_α under all motion cases show a good agreement with each other. Specifically, the ship section will experience the most significant upward hydrodynamic force around the time of $\xi = 0.75$ and then the force undergoes a steep drop until the end of water entry stage. In addition, if the ship section has a relatively greater

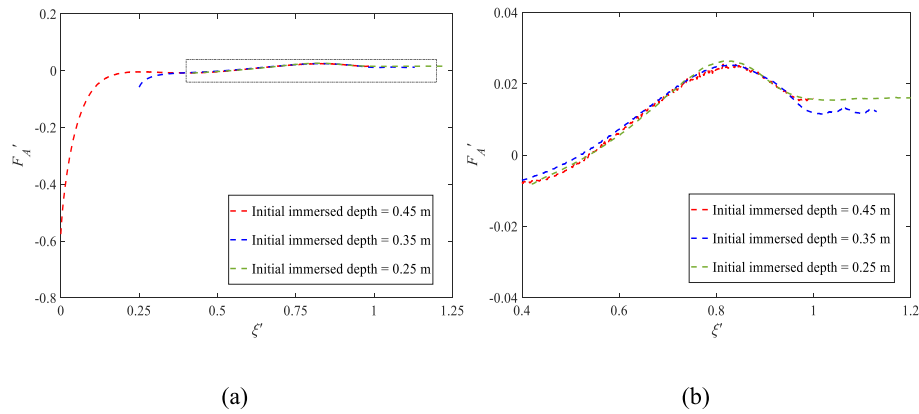


Fig. 10. Coefficient F_A' for the ship section model after manual scale and translation conducts. (a) The overall sketch; (b) The zoomed parts.

Table 8

Detailed information on motion cases for the ship section model under continuous water entry and exit with flow separation.

Model	Case No.	Constant acceleration	Immersion condition
Ship section model	34	$8 g \text{ m/s}^2$	0.45 m maximum penetration depth
	35		0.4 m maximum penetration depth
	36		0.35 m maximum penetration depth
	37	$5 g \text{ m/s}^2$	0.45 m maximum penetration depth
	38		0.4 m maximum penetration depth
	39		0.35 m maximum penetration depth
	40	$2 g \text{ m/s}^2$	0.45 m maximum penetration depth
	41		0.4 m maximum penetration depth
	42		0.35 m maximum penetration depth

maximum penetration depth, it will experience a greater supporting force and a smaller pulling force throughout the process. Furthermore, also expressing F_α as $F_\alpha = F_\alpha(\xi, h_m)$, we can partly overcome the limitation of the force decomposition approach by using the ship section model with the assumption of the specific maximum penetration depth, especially when the body moves with a large deceleration. In this case, the prediction of the total force acting on the body can be further facilitated.

(2) Without flow separation

The continuous water entry and exit of the ship section model without flow separation is then investigated. A total of six motion cases are given, the details of which are given in Table 9. Approximately 8.3 core hours are required to run each single simulation.

The extracted results of F_α are shown in Fig. 12. Unlike the wedge model A, even if the flow separation will never occur, the maximum penetration depth still has an influence on the evolution of F_α , but it is quite weak compared to the situation with the flow separation. Meanwhile, with respect to the tendency of F_α , a constant decreasing trend during the entry stage and a constant increasing trend during the exit stage can be observed from Fig. 12.

In general, the non-dimensional coefficient F_α for the ship section model is influenced by the penetration depth it can reach at the end of water entry and can be expressed accordingly as $F_\alpha = F_\alpha(\xi, h_m)$ whether or not flow separation occurs. However, fast and accurate force pre-

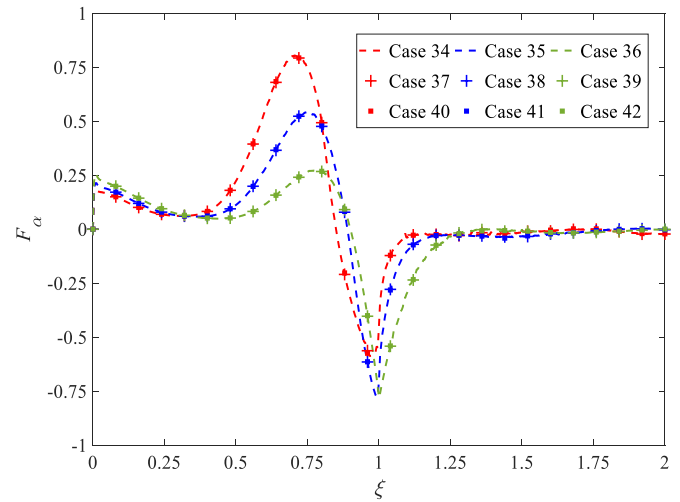


Fig. 11. Coefficient F_α for the ship section model with flow separation. (The specific type of line/symbol represents for the cases with the same constant acceleration while the specific colour represents those with the same immersion condition.)

dictions can still be provided under any specific motion case, but only if the maximum penetration depth is determined in advance.

4.5. Verification on the force decomposition approach

As shown in the previous subsections, the extraction results of the non-dimensional coefficients F_A and F_α respectively have a good

Table 9

Detailed information on motion cases for the ship section model under continuous water entry and exit without flow separation.

Model	Case No.	Constant acceleration	Immersion condition
Ship section model	43	$8 g \text{ m/s}^2$	0.25 m maximum penetration depth
	44		0.2 m maximum penetration depth
	45	$5 g \text{ m/s}^2$	0.25 m maximum penetration depth
	46		0.2 m maximum penetration depth
	47	$2 g \text{ m/s}^2$	0.25 m maximum penetration depth
	48		0.2 m maximum penetration depth

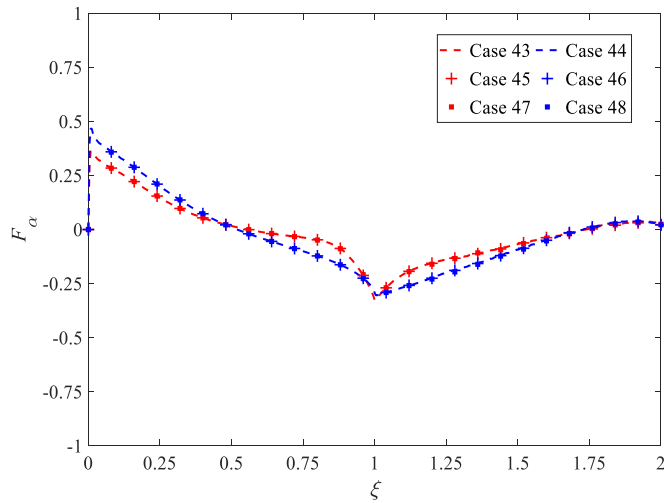


Fig. 12. Coefficient F_α for the ship section model without flow separation. (The specific type of line/symbol represents for the cases with the same constant acceleration while the specific colour represents those with the same immersion condition.)

agreement under certain motion cases. For the wedge model, these coefficients depend only on the displacement of body when considering direct water exit or continuous water entry and exit without the flow separation, and can be expressed as $F_A = F_A(\xi)$ and $F_\alpha = F_\alpha(\xi)$. As for the conditions involving the occurrence of flow separation or/and the body model of the complicated ship section, the immersion condition tends to have a considerable influence on these coefficients, in which case they should be written as $F_A = F_A(\xi, h_0)$ and $F_\alpha = F_\alpha(\xi, h_m)$. In short, by not taking into the details of the flow around the body, but by extracting these two non-dimensional coefficients, the force decomposition approach provides an effective way to predict the force acting on any body model, even those with complex shape contours.

In this subsection, the accuracy of the force decomposition approach for fast force prediction is investigated. The wedge model B and the ship section model are used as test models, which are given different motion cases. In addition to the constant acceleration cases, more complicated cases with varying accelerations are also included. The force predictions provided by the force decomposition approach are compared with results from available literature and/or direct CFD simulations. More details can be found in the following two parts.

(1) Wedge model B

The motion cases given to the wedge model B refer to the work of Piro and Maki (2011), who simulated the continuous water entry and exit of the same wedge by using another CFD software, OpenFOAM. More information on these motion cases can be found in Table 10. In detail, the wedge model B experiences two cases of continuous water entry and exit, case 49 and 50. Two different maximum penetration depths are 0.088 m (around the total height of the body) and 0.044 m (around half the total height of the body). Case 49 includes the occurrence of flow separation, whereas Case 50 does not.

As the finding in previous subsections, the motion state of body does

Table 10
Detailed information on tested motion cases for the wedge model B.

Model	Case No.	Constant acceleration	Immersion condition
Wedge model B	49	90.74 m/s ²	0.088 m maximum penetration depth
	50	181.48 m/s ²	0.044 m maximum penetration depth

not affect the extraction of F_α . First, in order to verify it, the results of F_α are extracted from two additional simulation cases, which correspond to the maximum penetration depth of 0.088 m and 0.044 m respectively, but both are with a constant acceleration of $8|g|$ m/s². The extracted profiles of F_α are shown in Fig. 13.

Subsequently, by using the force decomposition approach for continuous water entry and exit Eq. (15) together with the previously obtained F_α plotted in Fig. 13, the total forces acting on the body in cases 49 and 50 can be predicted in a fairly rapid manner without having to perform extensive numerical computations. The prediction results are compared with those obtained from the work of Piro and Maki (2011) and the direct STAR-CCM+ simulations, which can be observed in Fig. 14. It can be seen from Fig. 14 that the results from these three different methods are in good agreement with each other, in terms of both value and tendency. Although some slight discrepancies can be observed with the results between the force decomposition approach and OpenFOAM carried out by Piro and Maki (2011), the simulation results obtained by STAR-CCM+ have an almost perfect agreement with those obtained by our method. Therefore, the initial verification of the force decomposition approach has been completed with the promising result that our method is fully applicable to the motion case with arbitrary constant acceleration.

(2) Ship section model

The practical ship section model is then used for further verification. A total of three test motion cases are given to this model, the details of which are given in Table 11. Specifically, both direct water exit and continuous water entry and exit are considered, corresponding to Cases 51 and 52–53 respectively. Flow separation occurs in Case 52, but not in Case 53. Meanwhile, in order to verify the application of our proposed method on more complicated situations, in addition to a case with constant acceleration, cases with varying acceleration are also investigated (i.e. Case 52 and 53). The force prediction from our method will only be compared with those from direct STAR-CCM+ simulations.

All of the motion cases described in Table 11 have the same initial immersed depth or maximum penetration depth as described in Section 4.3 and 4.4. In this case, the extracted F_A with red colour in Fig. 9 can be used for Case 51, while the extracted F_α with blue colour in Fig. 11 and red colour in Fig. 12 can be used for Cases 53 and 52, respectively. The comparisons between the results by the force decomposition approach and by the direct STAR-CCM+ simulation are shown in Fig. 15. On the one hand, it can be seen in Fig. 15(a) that, for the direct water exit with constant acceleration, the prediction by the force decomposition

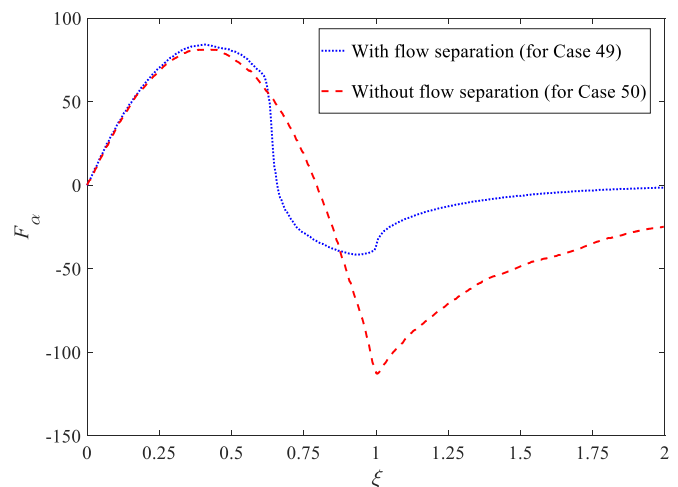


Fig. 13. Coefficient F_α for the wedge model B with and without flow separation.

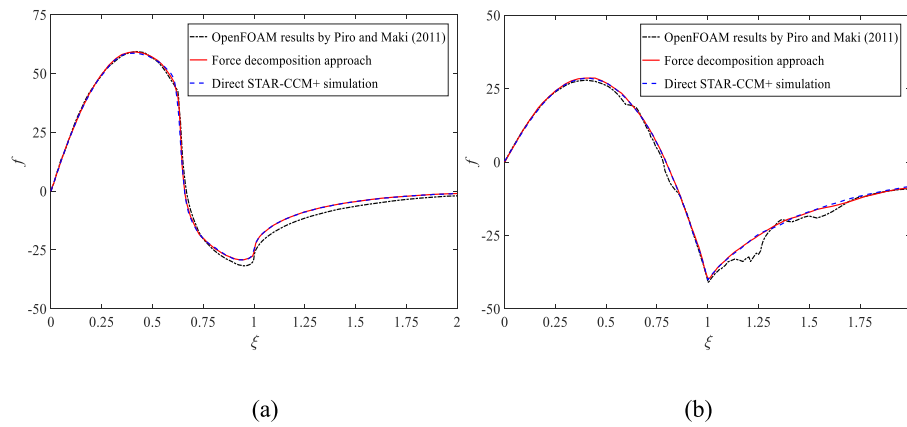


Fig. 14. Comparison of the total force acting on the wedge model B. (a) Case 49; (b) Case 50.

Table 11
Detailed information on test motion cases for the ship section model.

Model	Details		
Ship section model	The direct water exit		
	Case No.	Motion condition ($v_0 + at$)	Immersion condition
	51	$0 + 6 g t$ m/s	0.45 m initial immersed depth
	The continuous water entry and exit		
Case No.	Motion condition ($a = a(t)$)	Immersion condition	
52	$2 \times (1.46-t)$	0.4 m maximum penetration depth	
53	$2 \times (1.25-t)$	0.25 m maximum penetration depth	

approach shows an almost perfect agreement with that by the numerical method. On the other hand, with respect to the continuous water entry and exit with varying acceleration, our method still has a satisfactory performance. In detail, although some over-predictions can be clearly observed in Fig. 15(b) and (c) especially during the early stage of water entry, the force during the subsequent water exit stage and the evolution tendency of the whole process can still be described in a quite accurate way. Furthermore, for the limitation that the previous force decomposition approach cannot be applied to the deceleration circumstance, our method proposed in this paper provides an effective and reliable means to tackle this problem.

5. Conclusion

In this paper, the water entry and exit problem of a 2D rigid and symmetric body is investigated using the so-called force decomposition approach, as an extension of its application scope. The widely used wedge model and the complicated ship section model are used for the investigation. Two typical scenarios are considered, i.e. direct water exit and continuous water entry and exit. Based on the theoretical models available, the total force acting on the body can be approximated as a multiplication of several terms including the acceleration of body and the specific non-dimensional coefficients, i.e. F_A for direct water exit while F_a for continuous water entry and exit. Accordingly, the attention can be shifted to the calculation of F_A and F_a , if we do not focus much on the details of the flow around the body boundary. In order to investigate what plays a key role in these coefficients, each body model is given different motion cases with different constant acceleration and immersion conditions. To avoid the tedious calculation of the wetted boundary length of body, which tends to be very close to practical situations, CFD

methods are used here to numerically simulate these motion cases and then directly extract the results of F_A and F_a .

From our findings, it can be concluded that for a body model with a given shape contour, these two coefficients are only functions of the non-dimensional displacement and the immersion condition of body, i.e. $F_A = F_A(\xi, h_0)$ and $F_a = F_a(\xi, h_m)$. In addition, for the simple wedge models, the immersion condition seems to contribute little when the body experiences the direct water exit or the continuous water entry and exit without the occurrence of flow separation, in which case we can further obtain $F_A = F_A(\xi)$ and $F_a = F_a(\xi)$. Therefore, it can be expected that by using the force decomposition approach and the previously obtained non-dimensional coefficients, the force acting on a body of any shape can be provided in a fast way without extensive computational time for each particular case.

The accuracy of the force decomposition approach is further investigated. From the comparisons between the results obtained by the force decomposition approach and by direct CFD simulations, it is shown that our proposed method has a quite satisfactory performance both for the direct water exit and for the continuous water entry and exit. In addition, complicated motion cases with varying acceleration are also studied to evaluate the applicability of this method. It is a promising result that although over-predictions can be observed during the water entry stage, the discrepancies are limited and the force decomposition approach can still be used as an effective and reliable means to predict the total force acting on the body. After the successful verification, the method proposed in this paper is efficient to solve the problem of deceleration motion cases that fall into the limitation of the previous force decomposition approach.

However, as in the derivation performed in Section 2, the body velocity term, which is already present in the formula for calculating the total force, is neglected or converted to the part of the body acceleration term under the specific assumption. Therefore, our proposed method is unlikely to provide accurate force predictions when the body has a relatively fast velocity. Moreover, following the assumptions within analytical models that the duration of whole process is much shorter and that both gravity and viscosity of the fluid are ignored, our method also suffers from limitations when the movement of the body spans a longer period and/or the fluid is closer to the real one. The above factors affecting the applicability of our method deserve further research.

CRedit authorship contribution statement

Xupeng Sui: Writing – original draft, Validation, Resources, Methodology, Investigation, Data curation. **Kamal Djidjeli:** Writing – review & editing, Validation, Supervision, Resources, Formal analysis. **Zhe Sun:** Writing – review & editing, Supervision, Resources, Methodology, Formal analysis, Conceptualization. **Jing Tang Xing:** Writing – review & editing, Supervision.

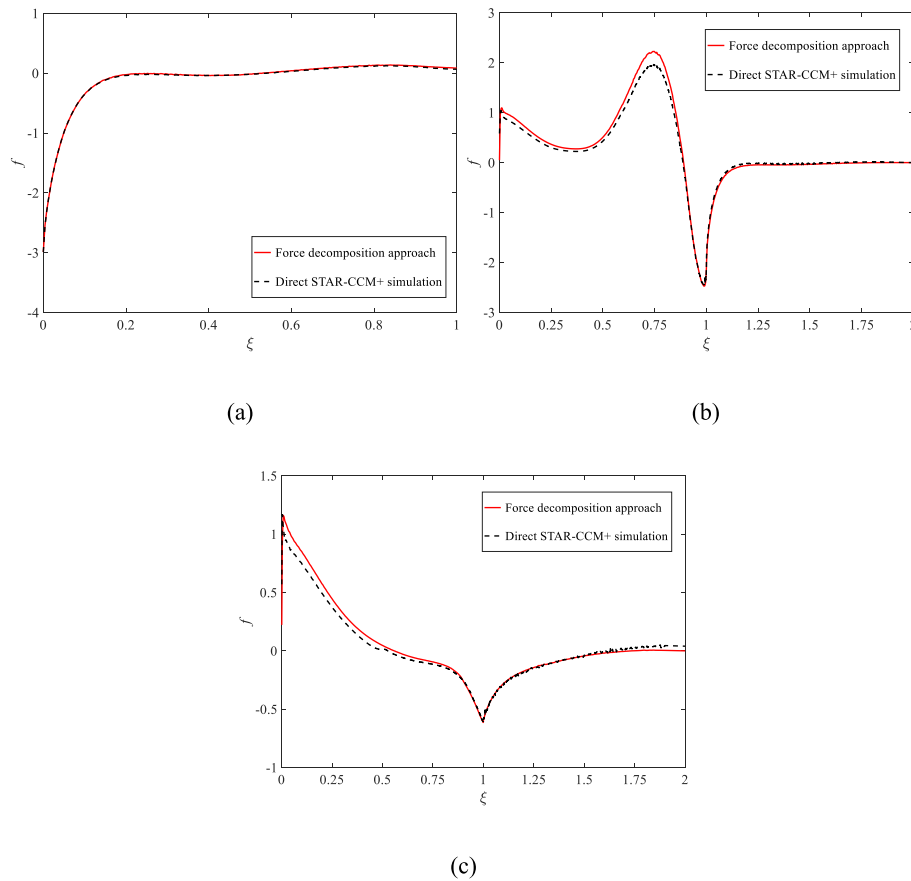


Fig. 15. Comparison of the total force acting on the ship section model. (a) Case 51; (b) Case 52; (c) Case 53.

Declaration of competing interest

The authors declare that they have no known competing financial interests or personal relationships that could have appeared to influence the work reported in this paper.

Data availability

Data will be made available on request.

Acknowledgments

This work is supported by the National Key Research and Development Program of China (2021YFC2801701 & 2021YFC2801700), National Natural Science Foundation of China (No. 52171295, 52192692), Fundamental Research Funds for the Central Universities (No. DUT22LK17), to which the authors are most grateful.

Appendix A. The force decomposition approach

The concept of force decomposition was originally proposed by Korobkin et al. (2014) who investigated the total force acting on the body entering water by observing several Wagner-type of theoretical models and then decomposed the force into two components, i.e. the body velocity and acceleration components. The detailed derivation is shown below. Further details can be found in Korobkin et al. (2014), Seng (2012) and Sun et al. (2022).

Within the entire solid-fluid domain, the fluid flow is still governed by the system of equations (Eq. 1). However, according to the Wagner-type models, the wetted boundary of body is treated as an equivalent flat disc during water entry, from which we can obtain

$$\varphi = -v\sqrt{c^2 - x^2} \quad (|x| < c(t)) \quad (\text{A. 1})$$

Then, the linearized Bernoulli equation $p = -\rho \times \partial\varphi/\partial t$ is used to calculate the pressure distribution along the wetted boundary of body, which gives

$$p(x, t) = \frac{\rho v c}{\sqrt{c^2 - x^2}} \frac{dc}{dt} + \rho \sqrt{c^2 - x^2} \frac{dv}{dt} \quad (\text{A. 2})$$

Then, by rewriting $c = c(h)$ as a function of the displacement of body and integrating the pressure along the entire wetted boundary, the total force can be expressed as

$$F(h) = \rho \pi v^2 c \frac{dc}{dh} + \rho \frac{\pi}{2} a c^2 \quad (\text{A. 3})$$

where the first term on the right hand in Eq. A.3 is called the body velocity component while the second term is called the body acceleration component. After further simplifying of Eq. A.3, we have

$$F(h) = \rho v^2 F_v(h) + \rho a F_a(h) \quad (\text{A. 4})$$

where $F_v(h)$ and $F_a(h)$ are two force coefficients that are not related to the motion state of body, but only to the displacement when the shape of body is specified. Therefore, given the contour and motion condition of body, the total force during water entry can be quickly predicted by using the pre-extracted force coefficients $F_v(h)$ and $F_a(h)$, which saves a lot of computational time. In general, there are two methods to extract $F_v(h)$ and $F_a(h)$, i.e. by theoretical calculation and by numerical simulation. The detailed procedure can be found in Korobkin et al. (2014) and Sun et al. (2022), respectively.

References

- Aarsnes, J.V., 1996. Drop Test with Ship Sections – Effect of Roll Angle. Norwegian Marine Technology Research Institute, Trondheim, Norway.
- Del Buono, A., Bernardini, G., Tassin, A., Iafra, A., 2021. Water entry and exit of 2D and axisymmetric bodies. *J. Fluid Struct.* 103.
- Faltinsen, O.M., 2005. *Hydrodynamics of High-Speed Marine Vehicles*. Cambridge University Press.
- Garne, K., 2005. Improved time domain simulation of planing hulls in waves by correction of the near-transom lift. *Int. Shipbuild. Prog.* 52, 201–230.
- Javed, A., Djidjeli, K., Xing, J., 2018. Low Reynolds number effect on energy extraction performance of semi-passive flapping foil. *J. Appl. Fluid Mech.* 11 (6), 1613–1627.
- Javed, A., Djidjeli, K., Xing, J., 2016. A coupled meshfree-mesh-based solution scheme on hybrid grid for flow-induced vibrations. *Acta Mech.* 227 (8), 2245–2274.
- Kaplan, P., 1987. Analysis and prediction of flat bottom slamming impact of advanced marine vehicles in waves. *Int. Shipbuild. Prog.* 34 (391), 44–53.
- Kaplan, P., 1992. Wave Impact Forces on Offshore Structures: Re-examination and New Interpretations, Offshore Technology Conference.
- Korobkin, A., 1996. *Water Impact Problems in Ship Hydrodynamics*. Computational Mechanics Publications, Southampton.
- Korobkin, A., 2004. Analytical models of water impact. *Eur. J. Appl. Math.* 15 (6), 821–838.
- Korobkin, A., Khabakhpasheva, T., Malenica, S., Kim, Y., 2014. A comparison study of water impact and water exit models. *Int. J. Nav. Archit. Ocean Eng.* 6 (4), 1182–1196.
- Korobkin, A.A., 2013. A linearized model of water exit. *J. Fluid Mech.* 737, 368–386.
- Korobkin, A.A., Khabakhpasheva, T.I., Maki, K.J., 2017. Hydrodynamic forces in water exit problems. *J. Fluid Struct.* 69, 16–33.
- Korvin-Kroukovsky, B.V., 1955. Investigation of ship motions in regular waves. *Trans. Soc. Nav. Archit. Mar. Eng.* 63, 386–435.
- Newman, J.N., 1964. A slender-body theory for ship oscillations in waves. *J. Fluid Mech.* 18 (4), 602–618.
- Newman, J.N., 2018. *Marine Hydrodynamics*. The MIT press.
- Newman, J.N., Sclavounos, P., Engineering, M.I.O.T.C.D.O.O., 1980. *The Unified Theory of Ship Motions*.
- Ogilvie, T.F., Tuck, E.O., 1969. *A Rational Strip Theory of Ship Motions: Part I*. University of Michigan.
- Paik, K.-J., Carrica, P.M., Lee, D., Maki, K., 2009. Strongly coupled fluid–structure interaction method for structural loads on surface ships. *Ocean Eng.* 36 (17–18), 1346–1357.
- Piro, D.J., Maki, K.J., 2011. Hydroelastic Wedge Entry and Exit, 11th International Conference on Fast Sea Transport, Honolulu, Hawaii, USA.
- Salvesen, N., Tuck, E., Faltinsen, O., 1970. *Ship Motions and Sea Loads*.
- Seng, S., 2012. *Slamming and Whipping Analysis of Ships*. Technical University of Denmark.
- Sun, F., Tan, M., Xing, J.T., 2012. Air-water two phase flow simulation using smoothed particle hydrodynamics. In: 2nd International Conference on Violent Flows. Editions Publibook, pp. 58–63.
- Sun, F., Tan, M., Xing, J.T., 2013. Application of incompressible smoothed particle hydrodynamics method for 3D fluid solid interaction problem. In: The 10th WSEAS International Conference on Fluid Mechanics (FLUIDS '13), Milan, Italy.
- Sun, Z., Djidjeli, K., Xing, J., 2017. The weak coupling between MPS and BEM for wave structure interaction simulation. *Eng. Anal. Bound. Elem.* 82, 111–118.
- Sun, Z., Djidjeli, K., Xing, J.T., Cheng, F., 2016. Coupled MPS-modal superposition method for 2D nonlinear fluid-structure interaction problems with free surface. *J. Fluid Struct.* 61, 295–323.
- Sun, Z., Jiang, Y.-c., Zhang, G.-y., Zong, Z., Xing, J.T., Djidjeli, K., 2019a. Slamming load on trimaran cross section with rigid and flexible arches. *Mar. Struct.* 66, 227–241.
- Sun, Z., Sui, X.P., Deng, Y.Z., Zou, L., Korobkin, A.A., Xu, L.X., Jiang, Y.C., 2021. Characteristics of slamming pressure and force for trimaran hull. *J. Mar. Sci. Eng.* 9 (6).
- Sun, Z., Sui, X.P., Korobkin, A., Zou, L., Zong, Z., 2022. Slamming force decomposition with gravity effect. *J. Fluid Struct.* 114.
- Sun, Z., Zhang, G.Y., Zong, Z., Djidjeli, K., Xing, J.T., 2019b. Numerical analysis of violent hydroelastic problems based on a mixed MPS-mode superposition method. *Ocean Eng.* 179, 285–297.
- Tassin, A., Piro, D.J., Korobkin, A.A., Maki, K.J., Cooker, M.J., 2013. Two-dimensional water entry and exit of a body whose shape varies in time. *J. Fluid Struct.* 40, 317–336.
- Von Karman, T., 1929. *The Impact on Seaplane Floats during Landing*. National Advisory Committee for Aeronautics, USA.
- Wagner, H., 1932. Über stoss-und gleitvorgänge an der Oberfläche von Flüssigkeiten. *Z. Angew. Math. Mech.* 12 (4), 193–215.
- Xing, J.T., 2019. *Fluid-Solid Interaction Dynamics: Theory, Variational Principles, Numerical Methods, and Applications*. Academic Press.
- Zhao, R., Faltinsen, O., Aarsnes, J., 1996. Water entry of arbitrary two-dimensional sections with and without flow separation. In: The 21st Symposium on Naval Hydrodynamics, Trondheim, Norway.